Available online at www.sciencedirect.com
ScienceDirect
Trans. Nonferrous Met. Soc. China 35(2025) 1394−1405
Transactions of Nonferrous Metals Society of China
www.tnmsc.cn

Microstructure, mechanical and thermo-physical properties of Al/Al−27%Si laminated composites

Zi-ming LI[1], Zhi-yong CAI[1,2], Hao YAN[1], Qian HAN[1], Nan CHEN[1], Ri-chu WANG[1,2], Xiang PENG[1], Chun ZHANG[3]

1. School of Materials Science and Engineering, Central South University, Changsha 410083, China;
2. National Key Laboratory of Science and Technology on High-strength Structural Materials, Central South University, Changsha 410083, China;
3. School of Chemistry and Materials Science, Hunan Agricultural University, Changsha 410128, China

Received 28 February 2025; accepted 25 April 2025

Abstract: Three types of Al/Al−27%Si laminated composites, each containing 22% Si, were fabricated via hot pressing and hot rolling. The microstructures, mechanical properties and thermo-physical properties of these composites were investigated. The results demonstrated that the three laminated composites exhibited similar microstructural features, characterized by well-bonded interfaces between the Al layer and the Al−27%Si alloy layer. The tensile and flexural strengths of the composites were significantly higher than those of both Al−22%Si and Al−27%Si alloys. These strengths increased gradually with decreasing the layer thickness, reaching peak values of 222.5 and 407.4 MPa, respectively. Crack deflection was observed in the cross-sections of the bending fracture surfaces, which contributed to the enhanced strength and toughness. In terms of thermo-physical properties, the thermal conductivity of the composites was lower than that of Al−22%Si and Al−27%Si alloys. The minimum reductions in thermal conductivity were 6.8% and 0.9% for the T3 laminated composite, respectively. Additionally, the coefficient of thermal expansion of the composites was improved, exhibiting varying temperature-dependent behaviors.

Key words: electronic packaging material; laminated composite; high-silicon aluminum alloy; mechanical property; thermo-physical property

1 Introduction

With the ongoing advancement of electronic devices towards integration, miniaturization, and high efficiency, electronic packaging materials, as an essential component of these devices, have garnered significant attention from scholars [1,2]. In response to complex operating environments and increasingly stringent packaging performance requirements, electronic packaging materials must possess not only an appropriate coefficient of thermal expansion (CTE) and high thermal conductivity, but also excellent mechanical properties to ensure reliable service performance [3−5].

Aluminum (Al) possesses several advantages, including high thermal conductivity, low density, and cost-effectiveness. However, it also has limitations such as relatively low strength, high CTE, and poor compatibility with packaged devices. By incorporating silicon (Si) as a reinforcement into the Al matrix, one can develop high-silicon aluminum alloys or Al/Si composites for electronic packaging applications. These alloys exhibit high thermal conductivity, low CTE, and low density [6−8]. In the 1990s, OSPREY Metal Co., Ltd. in the UK utilized spray deposition and hot isostatic pressing (HIP) to produce high-silicon

Corresponding author: Xiang PENG, Tel: +86-15601646388, E-mail: pengxiang@csu.edu.cn
https://doi.org/10.1016/S1003-6326(24)66756-7

aluminum alloys with Si content ranging from 22% to 90%. These alloys, known as controllable expansion (CE) alloys, exhibited superior machining, surface coating, and laser welding performance compared to Al/SiC_p and W/Cu composites [5]. The CTE of high-silicon aluminum alloys decreases as the Si content increases, leading to better compatibility with semiconductor chips like Si and GaSe. However, as the size of Si phase in the microstructure increases, it forms a network structure that enhances brittleness and reduces service reliability [9].

Laminated composites represent an advanced class of materials that integrate two or more distinct materials with varying properties into a layered architecture. These composites exhibit a "complementary effect", which not only mitigates the limitations of individual materials but also preserves and enhances their inherent advantages, thereby elevating the overall performance of the constituent materials [10−12]. Historical examples of laminated composites abound in ancient weaponry, including the undulating swords of medieval Europe, the renowned Damascus swords, Tang dynasty swords, and Japanese katana. Notably, the Shield of Achilles, dating back to 800 BC, exemplifies this technology with its intricate five-layer structure: bronze/tin/gold/tin/bronze. This sophisticated design rendered the shield virtually impenetrable even to the sharpest spears [13,14]. These findings indicate that the laminated composites have a long history of invention and application, and possess significant research value. In recent years, numerous studies have focused on fabricating composite materials through laminated composite technology to enhance their mechanical and thermophysical properties. GUO et al [15] fabricated a thick graphite/Sn laminated composite via welding technology, demonstrating a thermal flux twice that of the conventional metals such as Cu and Al, along with enhanced mechanical properties, thereby providing a solution for heat dissipation in integrated circuits. WANG et al [16] developed a Cu/CF(carbon fiber)/Cu sandwich structure, which was found to effectively enhance the in-plane thermal conductivity (TC) of CF/metal composites, showing promising applications in electronic packaging requiring highly directional heat transfer.

Laminated structures are advantageous for enhancing the strength and toughness of high-silicon aluminum alloys. During the fracture process of laminated composites under applied load, the layered architecture effectively inhibits crack propagation along the interfaces between layers upon reaching these interfaces. This inhibition prevents cracks from continuing in their original direction and mitigates fracture failure due to stress concentration. Moreover, incorporating intermediate layers with superior toughness can induce crack bifurcation and propagation within these layers, thereby significantly improving the overall toughness of the composite [17,18]. Moreover, during the preparation of laminated composites through processes such as hot pressing and hot rolling, dislocation accumulation and grain refinement occur, which significantly enhances the toughness [19]. In the Al/Al−Si laminated composites, the interfaces between layers effectively inhibit Si phase aggregation, thereby preventing or reducing the formation of a network structure, which in turn reduces the brittleness. Additionally, the interfaces between different Al−Si alloy layers impede crack propagation along the original path during fracture, contributing to a toughening effect. Furthermore, hot rolling of the laminated composite not only improves the intimate bonding between layers but also enhances the interfacial bonding strength. By controlling the deformation reduction, it is possible to achieve laminated composites with superior mechanical properties [20].

In this work, a laminated structure was obtained by alternately stacking Al−27%Si alloy sheets and Al foils, followed by hot pressing and hot rolling. The deformation reduction was controlled to regulate the layer thicknesses. The microstructures of the Al/Al−27%Si laminated composites were characterized, and their mechanical and thermo-physical properties were analyzed. Comparisons with the Al−22%Si alloy and the Al−27%Si alloy were conducted to investigate the effects of the laminated structure on mechanical properties, thermo-physical behavior, and fracture mechanisms.

2 Experimental

Al−27%Si and Al−22%Si alloys (all compositions are in mass fraction) were prepared

via nitrogen gas atomization and subsequently consolidated through hot pressing, as described in our previous study [21]. The Al−27% Si alloy was subjected to multi-pass hot rolling at 500 °C with a reduction of 6%−12% per pass and a holding time of 1 h to produce a 0.22 mm thick alloy sheet. These sheets and Al foils were subjected to surface cleaning. Subsequently, as shown in Fig. 1, they were alternately stacked with the alloy sheets positioned as the outermost layers. The stacks were configured to contain 19, 37, or 75 layers, respectively, and were subsequently hot pressed to form the laminated composites. These composites were further processed by multi-pass hot rolling to achieve a final thickness of 1.5 mm. The corresponding number of layers, thicknesses, and deformation reductions are summarized in Table 1. Hot pressing was conducted at 550 °C for 1 h, while hot rolling was performed at 500 °C with a holding time of 1 h, achieving a deformation rate of 6%−12% per pass.

Fig. 1 Schematic diagram of Al/Al−27%Si laminated composite structure

The Si contents in the laminated composites were measured using Inductively Coupled Plasma Optical Emission Spectrometry (ICP-OES), and the results are summarized in Table 1. Microstructures of the hot-rolled Al/Al−27%Si laminated composites were observed using an optical microscope (LEICA DM4M). Samples were etched with Keller's reagent at room temperature for 10−20 s, followed by ultrasonic cleaning in alcohol. The microstructure, phase composition, and fracture morphology of the Al/Al−27%Si laminated composites were analyzed in more details using a Quanta-200 environmental scanning electron microscope (SEM) equipped with energy-dispersive spectroscopy (EDS).

The density of the Al/Al−27%Si laminated composites was determined using the Archimedes displacement method. Room temperature tensile tests were performed on the laminated composites using an Instron 565 mechanical testing machine. The specimens were prepared with the dimensions illustrated in Fig. 2. The strain rate during these tests was set at 0.2 mm/min. Microhardness measurements were conducted using an HV-1000Z micro-Vickers hardness tester. The specimen surfaces were first polished with sandpaper and subsequently finished with diamond grinding paste to achieve a smooth surface. For each specimen, five measurements were taken and averaged. Room temperature three-point bending tests were conducted on the laminated composites using an MTS 858 electronic universal material testing machine. The test samples had dimensions of 12 mm × 4.5 mm × 1.5 mm, with a span length of 6 mm and a loading speed of 0.05 mm/min.

The CTE of the laminated composites was measured using a NETZSCH DIL 402 C dilatometer. The sample dimensions were 4 mm × 4 mm × 1.5 mm, and the testing temperature ranged from 30 to 400 °C. Thermal diffusivity was determined using a NETZSCH LFA 467 laser flash apparatus with samples in dimensions of 20 mm × 20 mm × 1.5 mm. Prior to testing, the sample surfaces were polished to a mirror finish using metallographic sandpaper. The thermal conductivity was then calculated using the following formula [22]:

$$c_p=\varphi_{\mathrm{Al}}c_{p,\,\mathrm{Al}}+\varphi_{\mathrm{Si}}c_{p,\,\mathrm{Si}} \tag{1}$$

$$\lambda=\alpha\rho c_p \tag{2}$$

where c_p is the specific heat capacity, φ_{Al} and φ_{Si} are the volume fractions of Al and Si respectively,

Table 1 Number of layers, thicknesses and deformation amounts of three kinds of Al/Al−27%Si laminated composites

Laminated composite	Thickness before hot rolling/mm	Thickness after hot rolling/mm	Thickness of Al layer/mm	Thickness of Al−27%Si alloy layer/mm	Number of layers	Si content in composite/ wt.%	Deformation reduction/ %
T1	2.5	1.5	0.03	0.132	19	22.22	40.0
T2	5.0	1.5	0.015	0.066	37	22.18	70.0
T3	10.0	1.5	0.0075	0.033	75	22.12	85.0

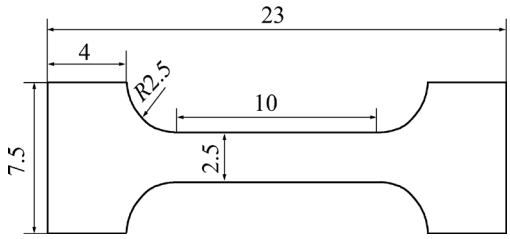

Fig. 2 Dimensions of tensile specimen (unit: mm)

$c_{p,\mathrm{Al}}$ and $c_{p,\mathrm{Si}}$ are the specific heat capacities of Al and Si respectively, λ is the thermal conductivity, α is the thermal diffusivity, and ρ is the density. All tests were conducted three times under identical conditions, and the average of the test results was calculated to ensure the accuracy and reliability of the experiment. The tensile strength, flexural strength, thermal conductivity and thermal expansion coefficient are the average values of three test results.

3 Results and discussion

3.1 Microstructural characteristics

Figure 3 illustrates the microstructure of the 0.22 mm thick Al−27%Si alloy sheet and three types of Al/Al−27%Si laminated composites. In the Al−27%Si alloy, only α-Al and β-Si phases are present, with the Si phase appearing in a granular form characterized by fine size and uniform distribution, as depicted in Fig. 3(a). Similarly, in all three types of Al/Al−27%Si laminated composites, only α-Al and β-Si phases are observed, and there is no significant difference in the size, morphology, or distribution of the Si particles. In the T1 laminated composite, a distinct and nearly straight interface between the Al layer and the Al−27%Si alloy layer is evident, as shown in Fig. 3(b). As the layer thickness decreases due to increased hot rolling reduction, the interlayer interface becomes increasingly indistinct and irregular, and the Al layer exhibits uneven thickness, as illustrated in Fig. 3(d).

Figures 4 and 5 present the EDS mapping and line scan results of the Al/Al−27%Si laminated composites. It is evident that the Si element predominantly resides in the Al−27%Si layer, with only a sparse distribution of Si particles in the Al layer, particularly in the T3 laminated composite. This phenomenon can be attributed to the significantly higher hardness of the Si phase compared to that of the Al phase, leading to some Si particles being embedded into the Al layer under compressive stress during hot rolling. The line scan results indicate excellent interfacial bonding between the Al layer and the Al−27%Si alloy layer. The thicknesses of the Al layers in the three laminated composites are approximately 29.73, 12.94, and 7.11 μm, respectively, closely matching the theoretical values. Additionally, no significant defects such as pores or micro-cracks are observed at the interlayer interface.

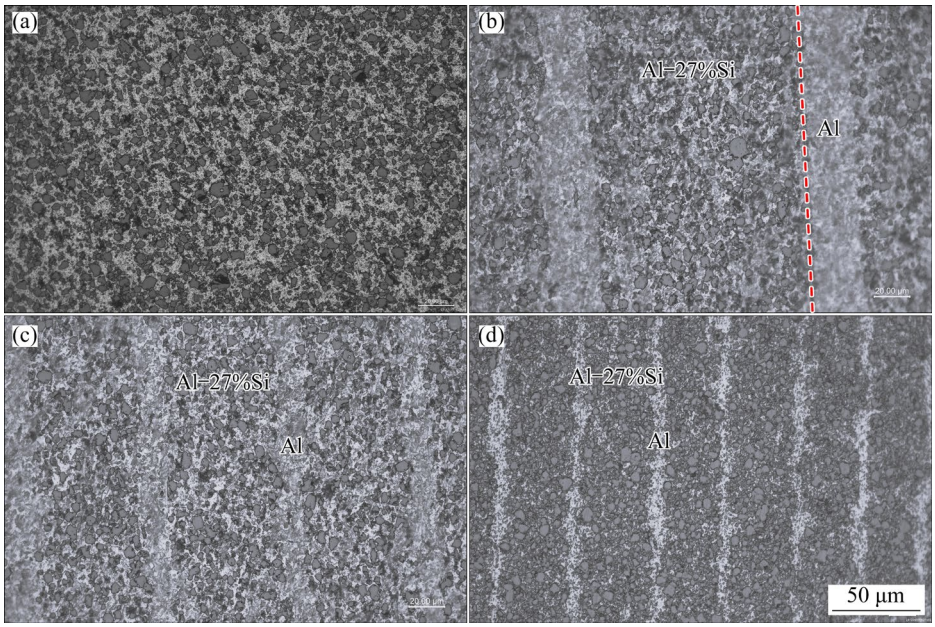

Fig. 3 Optical microstructures of Al−27%Si alloy sheet (a) and three kinds of Al/Al−27%Si laminated composites of T1 (b), T2 (c) and T3 (d)

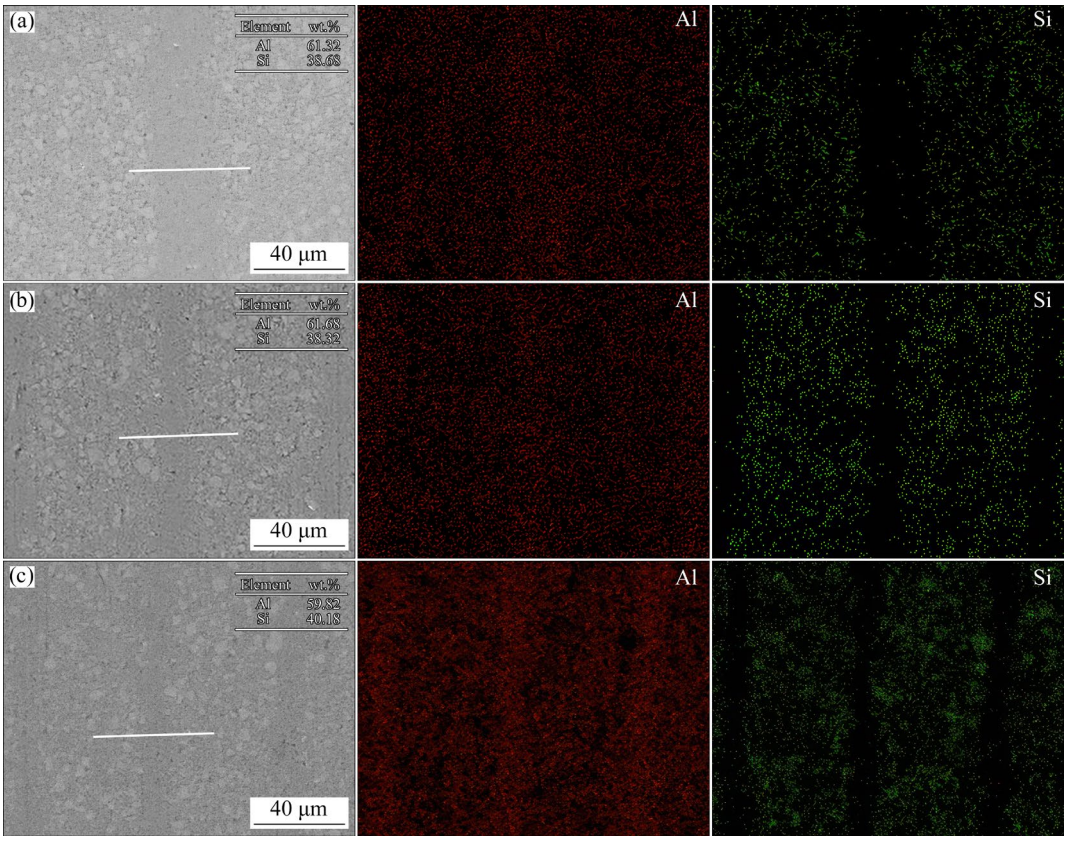

Fig.4 EDS mapping results of Al/Al−27%Si laminated composites: (a) T1; (b) T2; (c) T3

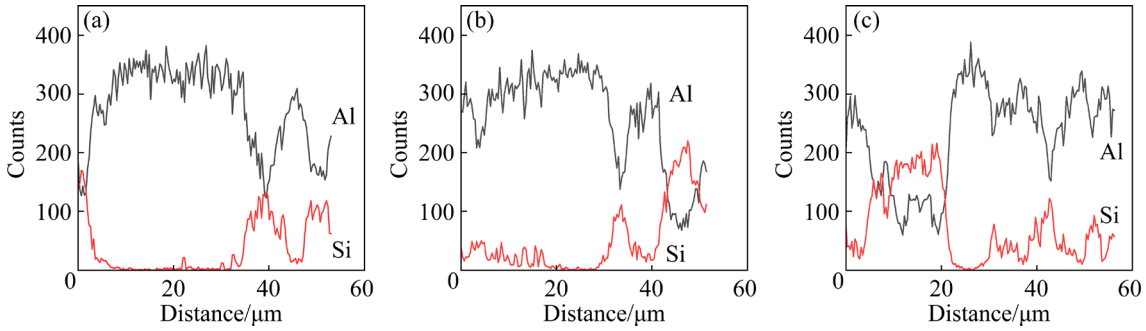

Fig. 5 EDS line scan results of Al/Al−27%Si laminated composites: (a) T1; (b) T2; (c) T3

The theoretical and measured densities of the Al/Al−27%Si laminated composites are presented in Table 2. The densities of the three laminated composites show minimal variation, with the relative densities reaching 99.2%, 99.5%, and 99.8% respectively. These high density levels suggest that the microstructures are highly compact, providing a solid foundation for their superior mechanical and thermo-physical properties [23].

Table 2 Measured density, theoretical density and relative density of Al/Al−27%Si laminated composites

Laminated composite	Experimental density/ ($g \cdot cm^{-3}$)	Theory density/ ($g \cdot cm^{-3}$)	Relative density/ %
T1	2.5878	2.6087	99.2
T2	2.5965	2.6095	99.5
T3	2.6057	2.6099	99.8

3.2 Mechanical properties

The average microhardness of the Al−22%Si alloy, and the Al−27%Si alloy layer in Al/Al−27%Si laminated composites is listed in Table 3. It can be seen that the hardness of Al−27%Si alloy layer significantly exceeds that of the Al−22%Si alloy. This difference can be attributed to the higher Si content and the increased residual stress induced

by hot rolling. However, the hardness of Al−27%Si alloy layer is slightly lower than that of Al−27%Si alloy. And as the thickness of Al−27%Si alloy layer decreases, its hardness gradually decreases. During hot rolling, the alloy undergoes plastic deformation, leading to a more homogeneous internal stress distribution, which reduces the residual stress within the composite material and consequently lowers the hardness of Al-27%Si alloy layer [24].

Table 3 Average hardness, room temperature tensile and flexural properties of Al−22%Si alloy, Al−27%Si alloy and Al/Al−27%Si laminated composites

Material	Vickers hardness (HV)	Tensile strength/ MPa	Elongation/ %	Flexural strength/ MPa
Al−22%Si	76.2	147.2	3.36	188.3
Al−27%Si	90.1	195.6	2.65	205.0
T1	89.1	215.4	2.73	368.0
T2	84.6	218.9	3.80	382.9
T3	80.5	222.5	3.88	407.4

Figure 6 illustrates the tensile stress−strain curves of the Al−22%Si alloy and the Al/Al−27%Si laminated composites. Table 3 summarizes the average tensile strength, elongation, and flexural strength for these materials. The tensile and flexural strength of the Al/Al−27%Si laminated composites are significantly higher than that of the Al−22%Si alloy and Al−27%Si alloy. Additionally, the elongation of the T2 and T3 laminated composites shows a slight improvement. With the decrease in the layer thickness, both tensile strength and elongation of the laminated composites exhibit a gradual increase. Specifically, the T3 laminated composite achieves peak values of 222.5 MPa in tensile strength and 3.88% in elongation. Moreover, the flexural strength of the T3 laminated composite reaches the highest value of 407.4 MPa. Compared with Al-22%Si and Al-27%Si alloy, the tensile strength and flexural strength of T3 composites are increased by 51.2%, 13.7% and 116.4%, 98.7%, respectively. Given that the elongation of the laminated composites is comparable to that of the Al−22%Si alloy and Al−27%Si alloy, while their tensile and flexural strength are significantly enhanced, it can be concluded that the toughness of the laminated composites surpasses that of the Al−22%Si alloy and Al−27%Si alloy.

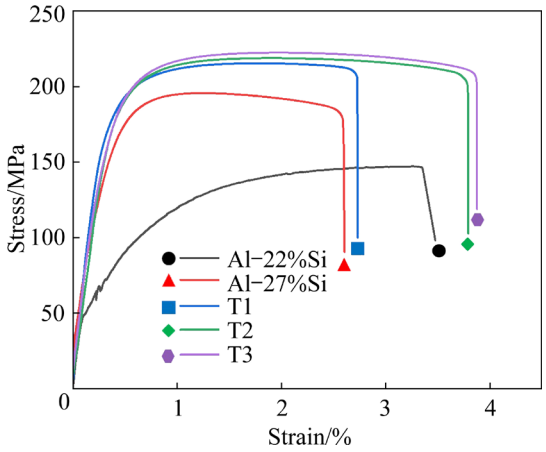

Fig. 6 Tensile stress−strain curves of Al−22%Si, Al−27%Si alloys and Al/Al−27%Si laminated composites at room temperature

The tensile fracture surfaces of the Al−22%Si alloy and the Al/Al−27%Si laminated composites are depicted in Fig. 7. In the Al−22%Si alloy, the relatively flat regions correspond to Si particles, which exhibit characteristic brittle fracture features; the surrounding dimples represent the Al matrix, indicating ductile fracture behavior. In the laminated composites, the Al−27%Si alloy layer displays a significant number of dimples alongside relatively flat regions, similar to the Al−22%Si alloy, suggesting ductile fracture of the Al matrix and brittle fracture of the Si particles. However, the size of the dimples is notably reduced, indicating a finer microstructure in the Al−27%Si alloy layer. The interfaces between the Al and Si phases in both the Al−22%Si alloy and the Al−27%Si alloy layer exhibit strong bonding, with no evidence of interfacial delamination or Si particle detachment. Additionally, the interface between the Al layer and the Al−27%Si alloy layer in the laminated composites shows excellent bonding, with no signs of interlayer delamination. These observations suggest that during tensile testing of the Al/Al−27%Si laminated composites, cracks propagate directly through the individual layers rather than along the interlayer interface.

With the decrease in layer thickness, the size of dimples in the Al/Al−27%Si laminated composites slightly decreases. During tensile deformation, cracks initiate in the less ductile Al−27%Si alloy layer. As these cracks propagate, their tips deflect, which effectively inhibits crack propagation. Upon reaching the more ductile Al layer, crack propagation

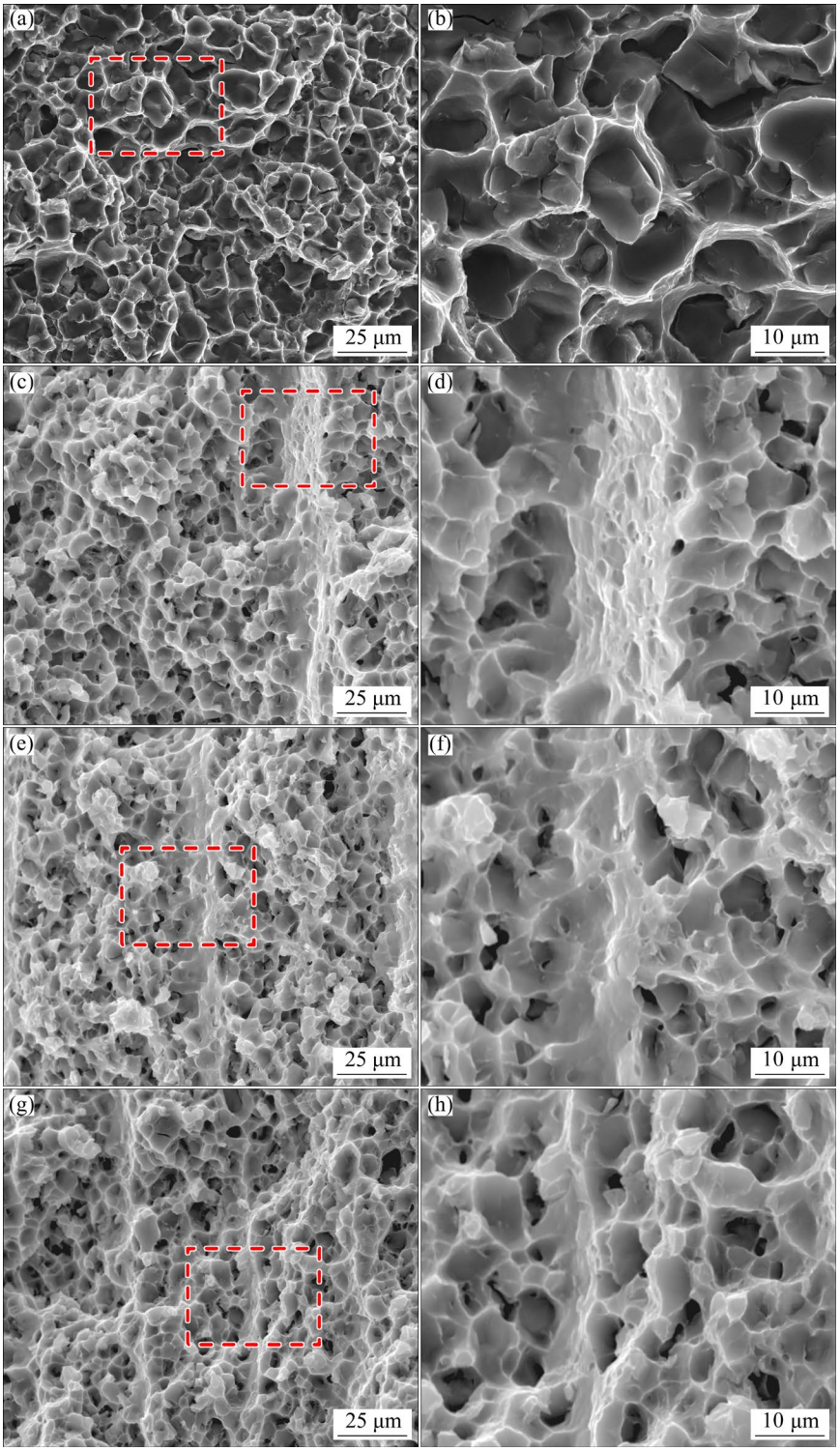

Fig. 7 Tensile fracture surfaces of Al−22%Si alloy and Al/Al−27%Si laminated composites: (a, b) Al−22%Si; (c, d) T1; (e, f) T2; (g, h) T3

is further impeded due to the superior toughness of the Al layer. The reduction in layer thickness leads to an increase in the number of Al layers, thereby enhancing the overall resistance to crack propagation and resulting in improved elongation. Moreover, during hot rolling, the alloy undergoes significant plastic deformation, leading to a finer and more homogeneous microstructure with an increased density of grain boundaries. This microstructural refinement enhances both the deformation resistance and the strength of the laminated composites [17].

The crack morphology of the three-point bending specimen of Al/Al−27%Si laminated composites is shown in Fig. 8. It is observed that during the bending test, the crack initiates in the outermost Al−27%Si alloy layer and deflects within this layer. Upon reaching the interface between layers, the crack does not propagate between layers but instead penetrates into the Al layer, where it deflects again. This observation further confirms the strong bonding strength between the Al layer and the Al−27%Si alloy layer in the laminated composites. The deflection of the crack during propagation increases the fracture surface area and the energy required for crack propagation, thereby effectively inhibiting fracture. Due to the superior toughness of the Al layer, when the crack enters this layer, its propagation is impeded, leading to increased elongation and enhanced strength. Consequently, as the layer thickness decreases and the number of Al layers increases, the toughening effect becomes more pronounced. In contrast, the bending cracks in Al−22%Si alloy specimens exhibit a nearly linear path.

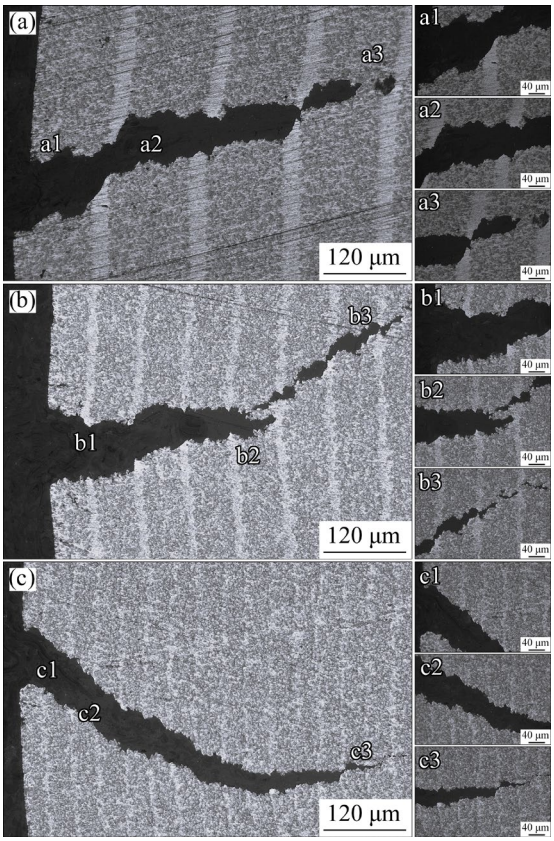

Fig. 8 Cross-sectional morphologies of bending specimens of Al/Al−27%Si laminated composites: (a) T1; (b) T2; (c) T3

3.3 Thermo-physical properties

The reinforcement in metal matrix composites is typically non-metallic. Factors influencing their thermal conductivity include the thermal conductivities of individual components, the volume fraction, size, shape, and distribution of the reinforcement, as well as the porosity and impurities [25,26]. The thermal conductivity of electronic packaging materials is a critical performance parameter. Higher thermal conductivity enhances the material's ability to dissipate heat from electronic components, thereby providing better protection.

The theoretical thermal conductivity can be calculated using the Maxwell model according to the following formula [27]:

$$\lambda_c=\lambda_m\frac{2\varphi_p\left(\frac{\lambda_p}{\lambda_m}-1\right)+\frac{\lambda_p}{\lambda_m}+2}{\varphi_p\left(1-\frac{\lambda_p}{\lambda_m}\right)+\frac{\lambda_p}{\lambda_m}+2} \tag{3}$$

where λ_c represents the theoretical thermal conductivity of the composite, λ_m is the thermal conductivity of the matrix, λ_p is the thermal conductivity of the reinforcement, and φ_p is the volume fraction of the reinforcement. The thermal conductivities of Al−22%Si alloy, Al−27%Si alloy and Al/Al−27%Si laminated composites were calculated by measuring their thermal diffusion coefficients.

Table 4 summarizes the theoretical and measured thermal conductivities of Al−22%Si alloy, Al−27%Si alloy and Al/Al−27%Si laminated composites. The measured thermal conductivities of all three Al/Al−27%Si laminated composites are consistently lower than their respective theoretical values. This discrepancy can be attributed to grain refinement during hot rolling, which increases the number of grain boundaries and dislocation density [24,28]. These microstructural evolutions impede atomic displacement within the grains, thereby reducing thermal conductivity. Additionally, the interlayer interfaces act as barriers to heat transfer, further diminishing the thermal conductivity of the laminated composites [29]. Consequently, as the layer thickness decreases, the interlayer interfaces become less distinct (as illustrated in Fig. 3), leading to an increase in thermal conductivity. Among the three laminated composites, the T3 composite exhibits the highest thermal conductivity of

166.5 W/(m·K), which is still 6.8% and 0.9% lower than that of the Al−22%Si and Al−27%Si alloy.

Table 4 Theoretical and measured thermal conductivities of Al−22%Si alloy, Al−27%Si alloy and Al/Al−27%Si laminated composites

Material	Theory thermal conductivity/ ($W·m^{-1}·K^{-1}$)	Experimental thermal conductivity/ ($W·m^{-1}·K^{-1}$)
Al−22%Si	215.3	178.6
Al−27%Si	202.7	168.0
T1	212.1	149.3
T2	212.3	153.1
T3	212.4	166.5

The high-silicon aluminum alloy and Al/Al−Si laminated composites consist of an aluminum matrix reinforced with Si phase particles. The addition of Si enhances the strength of the alloy while reducing its density. Since the thermal conductivity of Si (148 W/(m·K)) is lower than that of Al (237 W/(m·K)), the thermal conductivity of the alloy decreases as the Si content increases. In the laminated composites, the introduction of Al layers with superior thermal conductivity improves the overall thermal performance. Additionally, the thickness of the layers significantly influences the thermal conductivity; thinner layers may experience more complex interfacial structures during hot rolling, which can affect the thermal conduction differently.

The relationship between the CTE and temperature for Al−22%Si alloy and Al/Al−27%Si laminated composites is illustrated in Fig. 9. It is seen that the CTE of the three laminated composites increases sharply from room temperature to 100 °C, followed by a gradual increase with a relatively flat trend from 100 to 300 °C, and then exhibits a slight decrease between 300 and 400 °C. This thermal expansion behavior markedly differs from that of the Al−22%Si alloy and Al−27%Si alloy, which shows a nearly linear increase. Furthermore, as the layer thickness decreases, the CTE of the laminated composites also slightly decreases. These findings indicate that the laminated structure effectively reduces the CTE below temperatures 100 °C.

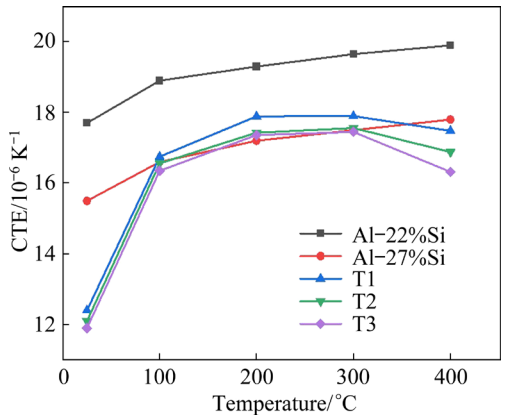

Fig. 9 Relationship between CTE and temperature for Al−22%Si alloy, Al−27%Si alloy and Al/Al−27%Si laminated composites

During the fabrication of laminated composites, residual stress arises at the interface boundary due to the differing CTE between the adjacent layers [30]. During hot rolling, the alloys experience plastic deformation, which balances the stress state at the interface and consequently reduces the residual stress. As the deformation reduction increases, the intensity of plastic deformation escalates, leading to a more significant reduction in residual stress. During thermal expansion, the residual stress within the composite is gradually released. Given that the T3 laminated composite undergoes the largest deformation, it exhibits the lowest residual stress. In the laminated composites, the Si phase within the Al−27%Si layer is segregated by the Al matrix. As the number of layers increases and the thickness of each layer decreases, the distribution of the Si phase becomes increasingly homogeneous. In the laminated composites, the Si phase in the Al−27%Si layer is separated by the Al layer. As the number of layers increases and the layer thickness decreases, the Si phase distribution becomes more homogeneous. However, the CTE of the Al matrix is significantly higher than that of the Si phase. During thermal expansion, the composite primarily expands due to the deformation of the Al matrix. With a more homogeneous distribution of Si, its restraining effect on the expansion of the Al matrix intensifies. Consequently, the CTE of the laminated composites decreases with decreasing layer thickness. When the temperature is relatively high (≥400 °C), the CTE of the laminated composites decreases. This can be attributed to the following reasons. (1) The gradual increase in the solid solubility of Si in the Al matrix leads to a reduction in the lattice constant of Al. Since the macroscopic length change rate of the material equals the lattice constant change rate,

this negatively impacts the thermal expansion behavior [31]. (2) During the expansion process, the tensile stress within the material gradually decreases and eventually transforms into compressive stress, thereby suppressing material expansion. (3) At the interface bonding regions, the constraining effect of the Si phase on the expansion of Al matrix strengthens, resulting in inhibited thermal expansion of the Al layers.

4 Conclusions

(1) By employing hot pressing and hot rolling techniques, Al/Al−27%Si laminated composites with excellent interlayer bonding between Al layer and Al−27%Si alloy layer were fabricated. However, despite their differences in layer thickness, the microstructures of these three laminated composites share some similarities. As the layer thickness decreases, the interlayer interface becomes less distinct, the uniformity of Al layer thickness decreases, and a small number of Si particles begin to infiltrate the Al layer.

(2) The tensile and flexural strengths of the three laminated composites are significantly higher than those of Al−22%Si and Al−27%Si alloys, and increase further as the layer thickness decreases. The maximum values reach 222.5 and 407.4 MPa, representing increases of 51.2%, 13.7% and 116.4%, 98.7%, respectively. Fracture surface analysis reveals distinct crack deflection phenomena, which contribute to the enhanced strength and toughness of the composites.

(3) Compared to the Al−22%Si alloy and Al−27%Si alloy, the thermal conductivity of the three laminated composites has decreased, with a minimum reduction of 6.8% and 0.9%. Increasing the deformation reduction and decreasing the layer thickness can improve the thermal conductivity. The thermal expansion behavior of the laminated composites differs from that of the alloy. The CTE of the composites is significantly lower than that of the Al−22%Si alloy, and approaches that of Al−27%Si alloy in the 100−400 °C range, and it exhibits a rapid increase from room temperature to 100 °C and slightly decreases at 400 °C.

CRediT authorship contribution statement

Zi-ming LI: Validation, Formal analysis, Investigation, Resources, Writing − Original draft, Review & editing; **Zhi-yong CAI:** Validation, Investigation, Writing − Review & editing; **Hao YAN:** Conceptualization, Writing − Revision, Supervision; **Qian HAN:** Conceptualization, Supervision, Validation, Formal analysis; **Nan CHEN:** Methodology, Investigation, Supervision, Conceptualization; **Ri-chu WANG:** Validation, Formal analysis, Writing − Review & editing, Funding acquisition, Resources; **Xiang PENG:** Writing − Review & editing, Visualization, Supervision; **Chun ZAHNG:** Writing − Review & editing, Visualization, Supervision.

Declaration of competing interest

The authors declare that they have no known competing financial interests or personal relationships that could have appeared to influence the work reported in this paper.

Acknowledgments

This work was supported by the National Natural Science Foundation of China (No. 52274369) and the National Key Laboratory of Science and Technology on High-strength Structural Materials, China (No. 623020034).

References

[1] ZOU Jin-xin, MA Chong, LIU Hui, CHANG Sha-sha, HONG Chun-fu, LIU Dong-guang, LUO Lai-ma. Exploration of pretreatment process and wettability of high bonding Ni−P coatings on W−Cu composites for electronic packaging [J]. Applied Surface Science, 2024, 673: 160911.

[2] YANG Qiu-guo, HUANG Ji-hua, CHEN Shu-hai, YE Zheng, WANG Wan-Li, YANG Jian. Influence of interfacial configuration on bonding properties and thermal conductivity of heterogeneous interface in Al/Graphite composite used for electronic packaging [J]. Surfaces and Interfaces, 2022, 35: 102452.

[3] SHAPIRO A A, TUDRYN C, SCHATZEL D, TSENG S. Electronic packaging materials for extreme, low temperature, fatigue environments [J]. IEEE Transactions on Advanced Packaging, 2010, 33(2): 408−420.

[4] WANG Xiao-zhen, SU Yi-shi, OUYANG Qiu-bao, ZHANG Di. Synergistic effects of tungsten coating on the microstructure, thermophysical and mechanical properties of graphite flakes reinforced copper matrix composites [J]. Journal of Alloys and Compounds, 2022, 916: 165318.

[5] GODBOLE K, BHUSHAN B, MURTY S V S N, MONDAL K. Al−Si controlled expansion alloys for electronic packaging applications [J]. Progress in Materials Science, 2024, 144: 101268.

[6] ZHOU Wei, WANG Ri-chu, PENG Chao-qun, CAI Zhi-yong. Microstructure and properties of Al−Si/Al−SiCp bilayer composite for electronic packaging [J]. Journal of Materials Science—Materials in Electronics, 2022, 33(10): 7811−23.

[7] ZHAO Xing-ming, MENG Jing-ran, ZHANG Chi, WEI Wei, WU Fu-fa, ZHANG Guan-gan. A novel method for improving the microstructure and the properties of Al−Si−Cu alloys prepared using rapid solidification/powder metallurgy [J]. Materials Today Communications, 2023, 35: 105802.

[8] MURAKAMI Y, FURUSHIMA R, SHIGA K, MIYAJIMA T, OMURA N. Mechanical property prediction of aluminium alloys with varied silicon content using deep learning [J]. Acta Materialia, 2025, 286: 120683.

[9] CAI Zhi-yong, ZHANG Chun, WANG Ri-chu, PENG Chao-qun, QIU Ke, FENG Yan. Preparation of Al−Si alloys by a rapid solidification and powder metallurgy route [J]. Materials & Design, 2015, 87: 996−1002.

[10] ZHANG Jia-chen, YANG Ming-nian, ZHAO Xin, CHEN Shuo-yan, TAO Dong, YAN Han-yang, HUANG Shi-xing, YANG Zhong. Microstructure and mechanical properties of Ti6Al4V-(TiC+TiB)/Ti laminated composites fabricated by hot press plus hot rolling [J]. Journal of Alloys and Compounds, 2025, 1014: 178674-.

[11] WANG S, XIE M Y, HUANG H B, KANG M, LIU R, CHEN C, ZHANG Z, ZHONG Z H, WU Y C. Diffusion behavior and bending fracture mechanism of W/Ti multilayer composites [J]. Journal of Alloys and Compounds, 2021, 879: 160451.

[12] YANG Wen-fan, GONG Ming-yu, YAO Jia-hao, WANG Jiang-wei, ZHENG Shi-jian, MA Xiu-liang. Hardening induced by dislocation core spreading at disordered interface in Cu/Nb multilayers [J]. Scripta Materialia, 2021, 200: 113917.

[13] WADSWORTH J, LESUER D R. Ancient and modern laminated composites — From the great pyramid of Gizeh to Y2K [J]. Materials Characterization, 2000, 45(4): 289−313.

[14] ALAMRY A. Fatigue damage and analysis of laminated composites: A state-of-the-art [J]. Journal of Engineering Research, 2024.

[15] GUO Wei-bing, HU Yi-ren, CHEN Xiao-guang, YUAN Ye, XUE Hai-tao, LI An-hang, FAN Chong. Super-thick highly thermally conductive graphite/Sn laminated composites assembled by active Ti-containing Sn−Ag−Ti filler metals [J]. Diamond and Related Materials, 2023, 138: 110253.

[16] WANG Zi-you, GAO Xian-peng, ZHANG Mu, SUN Xu-dong. The copper matrix composite with “sandwich” structure and three-dimensional networks, showcasing significantly improved thermal conducting performance [J]. Ceramics International, 2024, 50(17): 31097−31106.

[17] ZHANG Xuan-chang, WANG Cui-ju, DEN Kun-kun, NIE Kai-bo, GAN Wei-min, LIANG Wei, WU Yu-cheng. Fabrication, microstructure and mechanical properties of the as-rolled ZW31/PMMCs laminate [J]. Materials Science & Engineering A, 2019, 761: 138043.

[18] ZHAO Yan, LIU Jia-jing, ZHANG Yu-bo, SUN Xin, WANG Wei, LI Ting-ju. Achieving high strength, plasticity and conductivity in Cu/Cu-graphene oxide laminated composites with extremely low content of graphene oxide [J]. Materials & Design, 2025, 250: 113593.

[19] LI Zhen, WANG Xian-hui, ZHOU Sheng-yin, ZHANG Bo-chen, ZHANG Hong-bo, WANG Lei. Investigation on microstructure and strength-plasticity synergy mechanism of the laminated Mo2C@CNTs/Cu-20Mo composite [J]. Materials Characterization, 2025, 221: 114758.

[20] WANG Shuai, HUANG Lu-jun, LIU Bao-xi, PENG Hua-xin, JIAO Yang, GENG Lin. Microstructure and mechanical properties of Ti6Al4V based laminated composites at various rolling reductions [J]. Composites Communications, 2022, 33: 101212.

[21] CAI Zhi-yong, WANG Ri-chu, ZHANG Chun, PENG Chao-qun, WANG Lin-qian. Microstructure and properties of Al/Sip composites for thermal management applications [J]. Journal of Materials Science: Materials in Electronics, 2015, 26(6): 4234−4240.

[22] ZHENG Ze-yu, XU Hui, WEN Jia-lin, CHEN Ji-feng, MAO Zhu, ZHU Peng-li, SUN Rong, WU Wei-jing, PENG Jun-biao. In-situ growth of diamond/Ag as hybrid filler for enhancing thermal conductivity of liquid crystal epoxy [J]. Diamond and Related Materials, 2024: 141.

[23] ZHANG Yong-jian, PERSHIN L, YANG Zhen-ying, ZHANG Ya-hao, HAO Jin-peng, MOSTAGHIMI J, ZHANG Hai-long. Atmospheric plasma sprayed Cu coating on Cu−B/diamond composite for electronic packaging application [J]. Vacuum, 2024, 228: 113469.

[24] MA Jia-ji, DAI Yi-long, XU Xiang-chun, XU Xue-mei, FANG Hong-jie, LIU Hui, ZHANG Yu, YU Kun. Microstructures and properties of Al−27%Si composites: Influence of rolling and annealing [J]. Materials Transactions, 2018, 59(5): 724−729.

[25] CAI Zhi-yong, WEN Jing, WANG Ri-chu, FENG Yan, PENG Xiang, LI Xin-xing, LI Zi-ming, KANG Zhi-jie, ZHANG Xiao-di. Microstructure and properties of Cu/Si composites for electronic packaging: Effect of tungsten layer on silicon particles [J]. Journal of Alloys and Compounds, 2024, 997: 174847.

[26] LUO Jing, WANG Ri-chu, PENG Chao-qun, CAI Zhi-yong, FENG Yan, WANG Xiao-feng. Precipitation behavior and properties of Al−50Si−0.5X (X = Sc, La, Nb) alloys [J]. Journal of Materials Science: Materials in Electronics, 2022, 33(10): 7380−7395.

[27] OUYANG D L, WANG Z R, YANG T, ZHANG L W, WU D, CHEN W F, HU Q, GUO S. Cold sprayed Cu/Invar alloy composite [J]. Journal of Materials Research and Technology, 2025, 34: 2673−2683.

[28] WANG Hai-lu, WANG Guo-jun, HU Lian-xi, WANG Qiang, WANG Er-de. Effect of hot rolling on grain refining and mechanicalproperties of AZ40 magnesium alloy [J]. Transactions of Nonferrous Metals Society of China, 2011, 21(S2): s229−s234.

[29] ZHAN Ke, LI Feng-jia, LIU Jia-nan, CAO Jia-ming, WANG Zhuo, ZHAO Bin. Preparation and mechanism of Cu-GO laminated composite films with high thermal conductivity by intermediate nickel and silver layers via electrodeposition and ultrasonic spraying method [J]. Surface and Coatings Technology, 2023, 472: 1229960.

[30] ZHOU Wei, WANG Ri-chu, PENG Chao-qun, CAI Zhi-yong. Microstructure and properties of Al−Si functionally graded materials for electronic packaging [J]. Transactions of

Nonferrous Metals Society of China, 2023, 33(12): 3583−3596.
[31] HAHN T A, ARMSTRONG R W. Internal stress and solid solubility effects on the thermal expansivity of Al−Si eutectic alloys [J]. International Journal of Thermophysics, 1988, 9(2): 179−193.

Al/Al−27%Si 层状复合材料的显微组织、力学和热物理性能

李梓铭[1]，蔡志勇[1,2]，颜 豪[1]，韩 茜[1]，陈 楠[1]，王日初[1,2]，彭 翔[1]，张 纯[3]

1. 中南大学 材料科学与工程学院，长沙 410083；
2. 中南大学 高强结构材料科学与技术国家重点实验室，长沙 410083；
3. 湖南农业大学 化学与材料科学学院，长沙 410128

摘 要：采用热压和热轧制备三种 Al/Al−27%Si 层状复合材料(Si 含量均为 22%，质量分数)，对比研究其显微组织、力学性能和热物理性能。结果表明：三种复合材料具有相似的显微组织，Al 层与 Al−27%Si 合金层之间界面结合良好。三种复合材料的抗拉强度和抗弯强度均显著高于 Al−22%Si 和 Al−27%Si 合金，并随层厚减小而逐渐增大，最高分别达 222.5 和 407.4 MPa；弯曲试样的断口截面中可以观察到明显的裂纹偏转现象，这是层状复合材料强韧性提升的重要原因。与 Al−22%Si 合金和 Al−27%Si 合金相比，三种层状复合材料的热导率有所下降，其中 T3 层状复合材料的降幅最小，其热导率相较于 Al−22%Si 和 Al−27%Si 合金分别降低了 6.8%和 0.9%。复合材料的热膨胀系数也得到改善，并表现出不同的温度相关行为。

关键词：电子封装材料；层状复合；高硅铝合金；力学性能；热物理性能

(Edited by Sai-qian YUAN)